Perfect Brewster transmission by ultrathin perforated films

K. Pham[1], A. Maurel[2], J.-F. Mercier[3], S. Félix[4], M.L. Cordero[5], C. Horvath[5] and J.-J. Marigo[6]
[1]*IMSIA, ENSTA ParisTech - CNRS - EDF - CEA, Université Paris-Saclay, 828 Bd des Maréchaux, 91732 Palaiseau, France.*
[2]*Institut Langevin, ESPCI ParisTech, CNRS UMR 7587, 1 rue Jussieu, 75005 Paris, France.*
[3]*Poems, CNRS, ENSTA ParisTech, INRIA, 828 Bd des Maréchaux, 91762 Palaiseau, France.*
[4]*LAUM, CNRS UMR 6613, Le Mans Université, av. Olivier Messiaen, 72085 Le Mans, France.*
[5]*Departamento de Física Facultad de Ciencias Físicas y Matematicas, Universidad de Chile, Av. Blanco Encalada 2008, Santiago, Chile. and*
[6]*Lab. de Mécanique des Solides, Ecole Polytechnique, Route de Saclay, 91120 Palaiseau, France.*

We address the perfect transmission of a plane acoustic wave at oblique incidence on a perforated film, being sound penetrable or rigid. It is shown that the Brewster incidence θ^* realizing a so-called extraordinary transmission is significantly shifted when the thickness of the film becomes subwavelength. To account for subwavelength thicknesses, an interface model is proposed which differs from the classical one based on effective medium theory. This interface model is able to reproduce with high accuracy the overall spectra of ultra-thin to relatively thick perforated films. Depending on the contrasts in the material properties of the film and of the surrounding matrix, decreasing the film thickness can produce an increase or a decrease of θ^*; it can also produce the disappearance of a perfect transmission or, to the contrary, its appearance.

I. INTRODUCTION

Extraordinary optical/acoustical transmission (EOT/EAT) refers to high transmission through films with subwavelength apertures (Fig. 1), while a single aperture would transmit light/sound very poorly [1]. This means that such a transmission is possible because of collective effects of the holes. These collective effects can make the perforated film able to support surface waves as it has been primarily observed on plasmonic structures by Ebbesen [2] or able to support resonances of the Fabry-Perot type [3, 4]. They can be non resonant when they lend to the film an effective impedance which matches that of the surrounding matrix at the so-called Brewster incidence [5, 6]. The tunability of the Brewster angle has been exemplified by means of the geometrical parameters of perforated rigid screens [7, 8] and exploited to realize beam shifter [9] and flat lenses [10]; its tunability with the material properties of sound penetrable films has been studied in [11] and exemplified in [12] and in [13] where absorber devices with low-loss have been proposed. Eventually, and in contrast with resonance based mechanisms, EOT at the Brewster angle has the advantage to be mildly affected by the losses [14].

From a theoretical point of view, perfect transmissions have been analyzed owing to effective medium theories based on classical homogenization, which predicts that the perforated film can be replaced by an equivalent homogeneous one for which the scattering properties are explicit. Such approaches have been applied firstly to sound-rigid films [15, 16] and their electromagnetic counterparts [5, 17] and it has been generalized to more involved geometric perforations [7, 8] and to sound-penetrable films [11, 12]. By construction, effective medium theories aim to describe the effective propagation within the film and disregard the evanescent field excited at its ending boundaries. Intuitively, this is sounding if the film is thick enough to ensure that the effect of wave propagation is dominant compared to that of the boundary layers. When this is not the case, other strategies of homogenization have to be sought. Examples are structured devices in which both effects have to be accounted for [18, 19] or in which the boundary layer effects become dominant [20–22]. The realization of ultra-thin devices with unusual scattering properties is appealing and it makes sense to determine if the properties observed for relatively thick devices live on for thin ones. We know that perfect transmission based on Fabry-Perot resonances will disappear in this limit; but it is less intuitive to say if perfect transmission of the Brewster type can survive. To anticipate on this question, Fig. 2 reports the variation of $|R|$ against the incidence θ and the dimensionless film thickness e/h. In the three reported cases for sound penetrable and sound rigid films, the Brewster angle θ^* realizing perfect transmission appears to vary with e/h, a fact which cannot be explained by the matching impedance condition invoked by the

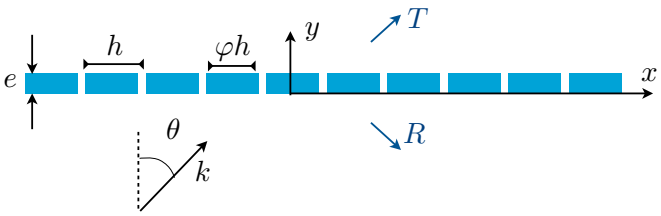

FIG. 1: Scattering of an acoustic wave at oblique incidence θ on a perforated film. The mass densities and sound velocities are $(\rho_\mathrm{i}, c_\mathrm{i})$ in the film material and $(\rho_\mathrm{m}, c_\mathrm{m})$ in the matrix; $k = \omega/c_\mathrm{m}$ is the wavenumber in the matrix.

classical homogenization. We shall see that the interface homogenization focusing on the effect of the evanescent field accurately recovers these scattering properties.

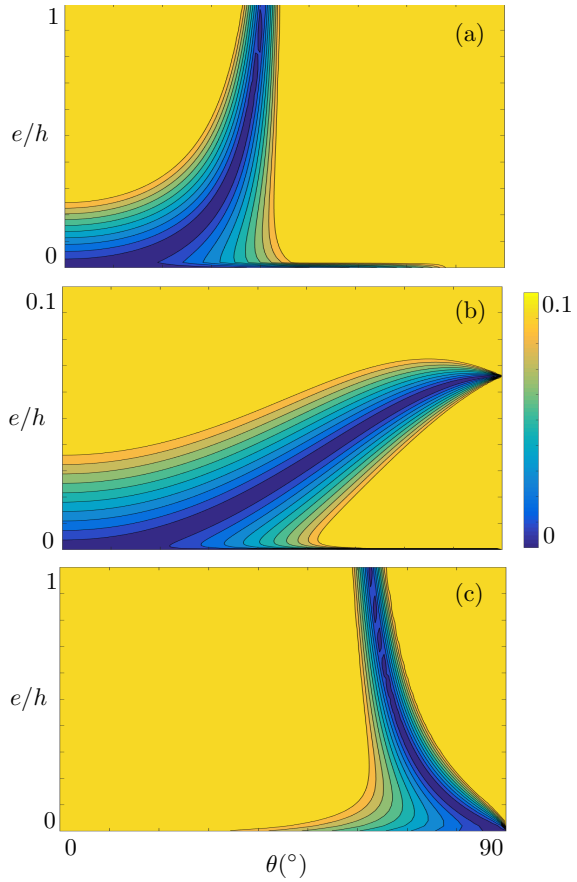

FIG. 2: Perfect transmission at the Brewster angle. Reflection $|R|$ computed numerically (in colorscale with saturation for $|R| > 0.1$) against the incidence θ and the film thickness e/h ($\varphi = 0.5$) (a) with $\rho_{\rm i}/\rho_{\rm m} = 10^{-3}$ and $\chi_{\rm i}/\chi_{\rm m} = 1$, (b) with $\rho_{\rm i}/\rho_{\rm m} = 10^{-3}$ and $c_{\rm i} = 10c_{\rm m}$ and (c) for a sound rigid perforated film.

The paper is organized as follows. In Section II, the classical effective medium predictions for the scattering coefficients (R, T), Eq. (6), and for the resulting Brewster incidence $\theta_{\rm B}$, Eq. (8), are recalled. We also provide the predictions given by the effective interface model detailed in [22] : (R, T) in (12) and the resulting Brewster angle θ^* in (14). The value of θ^*, when it exists, is given by effective interface parameters which depend on the film thickness, and its variations when going from thin to thick films are inspected in Section III. For sound penetrable films, we use explicit expressions of the interface parameters in the limiting cases $e/h \to 0$ and $e/h \to \infty$ to discuss on the existence of a perfect transmission depending on the material properties of the film; when perfect transmission is possible, explicit expressions are provided, Eqs. (17). The case of sound-rigid film is also considered as a particular case of sound- penetrable film; in this case, approximate expressions of the interface parameters are provided for any film thickness, Eqs. (18). It is shown that our findings quantitatively explain the spectra of Fig. 2 with high accuracy. We collect in Appendix A additional informations on the interface parameters.

II. EFFECTIVE MEDIUM AND INTERFACE MODELS

We consider propagation of acoustic waves in the harmonic regime with time dependence $e^{-i\omega t}$. The propagation is described by the Euler equations for the pressure p of the form

$$\mathrm{div}\left(\frac{1}{\rho(\mathbf{x})}\boldsymbol{\nabla} p\right) + \omega^2 \chi(\mathbf{x})\, p = 0, \tag{1}$$

with the mass density $\rho(\mathbf{x})$ and the isentropic compressibility $\chi(\mathbf{x})$ varying in space $\mathbf{x} = (x, y)$, see Fig. 1. In the perforated film they are denoted $\rho_{\rm i}$ and $\chi_{\rm i} = 1/(\rho_{\rm i} c_{\rm i}^2)$, with $c_{\rm i}$ the sound speed; in the surrounding matrix, they are denoted $\rho_{\rm m}$ and $\chi_{\rm m} = 1/(\rho_{\rm m} c_{\rm m}^2)$. With $k = \omega/c_{\rm m}$ the incident wavenumber, the wave propagation in the matrix is described by the Helmholtz equation

$$\Delta p + k^2 p = 0, \qquad y < 0 \text{ and } y > e, \tag{2}$$

and effective models aim at simplifying the effect of the propagation in the inhomogeneous region $0 < y < e$. In the classical effective medium model, this is done by replacing this region by a homogeneous and anisotropic one; in the effective interface model, this is done by imposing non intuitive jump conditions between $x = 0$ and $x = e$.

A. Classical effective medium model

The classical model is based on effective medium theory (or classical homogenization); it tells us that a medium made of layers can be replaced by an equivalent homogeneous and anisotropic medium described by the wave equation

$$\mathrm{div}\left(\begin{pmatrix} \rho_{\rm m}/\rho_x & 0 \\ 0 & \rho_{\rm m}/\rho_y \end{pmatrix} \boldsymbol{\nabla} p\right) + \chi_{\rm r}\, k^2 p = 0, \quad 0 < y < e, \tag{3}$$

involving effective mass densities (ρ_x, ρ_y) and a relative effective compressibility $\chi_{\rm r}$ defined by

$$\begin{cases} \dfrac{\rho_{\rm m}}{\rho_y} = \varphi \dfrac{\rho_{\rm m}}{\rho_{\rm i}} + 1 - \varphi, & \dfrac{\rho_x}{\rho_{\rm m}} = \varphi \dfrac{\rho_{\rm i}}{\rho_{\rm m}} + 1 - \varphi, \\ \chi_{\rm r} = \varphi \dfrac{\chi_{\rm i}}{\chi_{\rm m}} + (1 - \varphi). \end{cases} \tag{4}$$

Within this description, the film is replaced by a layer of thickness e where (3) applies surrounded by the matrix where (2) applies. For an incident plane wave at

incidence θ, the solution reads

$$p(\mathbf{x}) = e^{i\alpha x}\begin{cases} \left(e^{i\beta y} + R\, e^{-i\beta y}\right), & y<0, \\ \left(A\, e^{iKy} + B\, e^{-iKy}\right), & 0<y<e, \\ T\, e^{i\beta(y-e)}, & y>e \end{cases} \tag{5}$$

with $\alpha = k\sin\theta$, $\beta = k\cos\theta$. Applying at $y = 0, e$ the conditions of continuity of the pressure and of the normal velocity u_y ($u_y = \frac{1}{\rho_y}\partial_y p$ in the effective film and $u_y = \frac{1}{\rho_{\rm m}}\partial_y p$ in the matrix) provides the scattering coefficients of the form

$$\begin{aligned} R &= \frac{2i(\xi^2-1)\sin Ke}{(\xi-1)^2 e^{iKe} - (\xi+1)^2 e^{-iKe}}, \\ T &= \frac{4\xi}{(\xi-1)^2 e^{iKe} - (\xi+1)^2 e^{-iKe}}, \end{aligned} \tag{6}$$

with

$$K = k\sqrt{\frac{\rho_y \chi}{\rho_{\rm m}\chi_{\rm m}} - \frac{\rho_y}{\rho_x}\sin^2\theta}, \quad \xi = \frac{\rho_y}{\rho_{\rm m}}\frac{k\cos\theta}{K}. \tag{7}$$

The Brewster incidence $\theta_{\rm B}$ realizing perfect transmission independently of the frequency k corresponds to the condition of impedance matching, $\xi = 1$, that is

$$\cos\theta_{\rm B} = \sqrt{\frac{\rho_{\rm m} - \chi_{\rm r}\,\rho_x}{\rho_{\rm m} - \rho_x\rho_y/\rho_{\rm m}}}. \tag{8}$$

Eventually, perfect transmission due to Fabry-Perot resonances is also obtained for $Ke = \pi/2 + n\pi$; this corresponds to constructive interferences during wave propagation in the film and as previously said, it requires sufficient large film thickness e.

B. Effective interface model

The effective model based on homogenization of thin interface has been developed in [22]. It aims at capturing the boundary layer effects due to the evanescent field excited at the end boundaries of the perforated film. Because of the low frequency regime, the evanescent field ressembles that of a static field associated with the Laplace equation which allows us to reduce its effect to effective, though non intuitive, transmission conditions. These conditions tell us that the pressure and the normal velocity are not continuous but they experience jumps which read

$$\begin{cases} [\![p]\!]_e = h\mathcal{B}\,\dfrac{\partial \overline{p}}{\partial y}, \\ \left[\!\!\left[\dfrac{\partial p}{\partial y}\right]\!\!\right]_e = -h\mathcal{C}\,\dfrac{\partial^2 \overline{p}}{\partial x^2} - h\mathcal{D}k^2\,\overline{p}, \end{cases} \tag{9}$$

where we have defined for any field f

$$[\![f]\!]_e \equiv f(e,x) - f(0,x), \quad \overline{f} \equiv \frac{1}{2}\left[f(e,x) + f(0,x)\right]. \tag{10}$$

Among the 3 interface parameters entering in the jump conditions, $\mathcal{D}$ is explicit, see forthcoming (15), while $(\mathcal{B},\mathcal{C})$ are deduced from static problems and in general, they have to be determined numerically (see Appendix A). However, we shall see that they have explicit expressions in the limit of thin and thick film corresponding to small and large e/h values, see forthcoming (16).

Within this description, the perforated film has been replaced by a region $y \in (0,e)$ across which (9) applies; it is worth noting that the interior region does not need to be specified, the jump conditions being sufficient to link the behavior of the wave in the matrix at $y = 0$ and $y = e$. Hence, the solution of the scattering problem now reads

$$p(\mathbf{x}) = e^{i\alpha x}\begin{cases} e^{i\beta y} + Re^{-i\beta y}, & y<0, \\ Te^{i\beta(y-e)}, & y>e. \end{cases} \tag{11}$$

Applying the jump conditions (9) provides the scattering coefficients of the form

$$R = \frac{1}{2}\left(\frac{z_1}{z_1^*} - \frac{z_2}{z_2^*}\right), \quad T = \frac{1}{2}\left(\frac{z_1}{z_1^*} + \frac{z_2}{z_2^*}\right), \tag{12}$$

with

$$\begin{cases} z_1 = 1 + \dfrac{ikh}{2}\mathcal{B}\cos\theta, \\ z_2 = 1 + \dfrac{ikh}{2\cos\theta}\left(\mathcal{D} - \mathcal{C}\sin^2\theta\right). \end{cases} \tag{13}$$

From (12), perfect transmission is expected at an incidence θ^* satisfying

$$\cos\theta^* = \sqrt{\frac{\mathcal{C}-\mathcal{D}}{\mathcal{C}-\mathcal{B}}}, \tag{14}$$

and we shall see that θ^* in general differs from the classical prediction $\theta_{\rm B}$ in (8). Expectedly, the effective interface model is unable to predict resonances of the Fabry-Perot type that is occurring at a prescribed frequency whatever the incidence is. This is because the film is assumed to be very thin, and notably too thin to satisfy a quarter wavelength criterion.

III. VARIATION OF THE BREWSTER ANGLE FOR THIN FILMS

We now move on to the analysis of the results reported in Fig. 2. To get insights of the scattering properties of ultrathin films, it is useful to inspect the limiting cases of small/large thicknesses e/h, for which we shall see that explicit expressions of the interface parameters $(\mathcal{B},\mathcal{C})$ are available.

A. Limiting cases of thin/thick films

As previously said, among the 3 parameters entering in the jump conditions (9), only $\mathcal{D}$ is explicit with

$$\mathcal{D} \equiv \chi_{\rm r}\,\frac{e}{h}, \tag{15}$$

with $\chi_{\rm r}$ defined in (4), while $(\mathcal{B},\mathcal{C})$ require the resolution of static problems. However, it is possible to establish bounds for $(\mathcal{B},\mathcal{C})$ which will prove useful. In [22], lower bounds were established and we provide in the Appendix A the derivation of the upper bounds, which eventually leaves us with

$$\frac{\rho_y}{\rho_{\rm m}}\,\frac{e}{h} \le \mathcal{B} \le \frac{\rho_x}{\rho_{\rm m}}\,\frac{e}{h}, \qquad \frac{\rho_{\rm m}}{\rho_x}\,\frac{e}{h} \le \mathcal{C} \le \frac{\rho_{\rm m}}{\rho_y}\,\frac{e}{h}, \tag{16}$$

where (ρ_x,ρ_y) are the geometrical and arithmetical averages of the mass densities defined in (4) and entering in the classical effective medium model. Now, we shall make use of these explicit bounds to inspect the variations of the Brewster angle θ^* in (14). To do so, it is sufficient to remark that $(\mathcal{B},\mathcal{C})$ reach their upper bounds for vanishing thickness e/h and their lower bounds for large e/h, as illustrated in Fig. 3. It follows that inserting (16) in

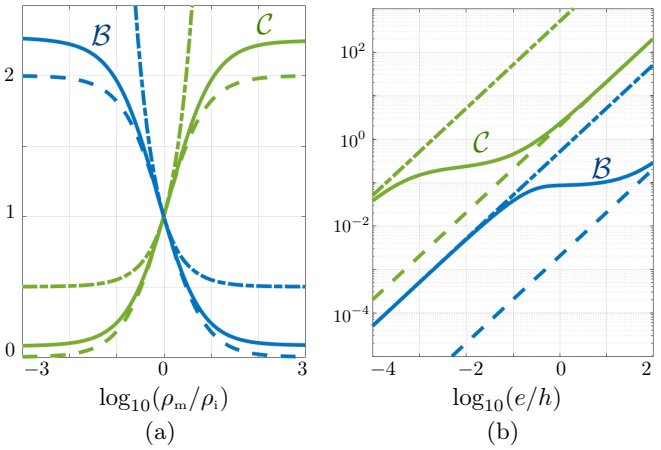

FIG. 3: Interface parameters $\mathcal{B}$ (plain blue line) and $\mathcal{C}$ (plain green line) for $\varphi = 0.5$ (a) against $\log_{10}(\rho_{\rm m}/\rho_{\rm i})$ for $e/h = 1$ and (b) against $\log_{10}(e/h)$ for $\rho_{\rm m}/\rho_{\rm i} = 10^3$. In (a-b), the dashed and the dashed-dotted lines shows the lower and upper bounds (16).

(14) gives

$$\begin{cases} \text{for thin films, } \cos\theta^* = \sqrt{\dfrac{\rho_{\rm m} - \chi_{\rm r}\,\rho_y}{\rho_{\rm m} - \rho_x\rho_y/\rho_{\rm m}}}, \\ \text{for thick films, } \cos\theta^* = \sqrt{\dfrac{\rho_{\rm m} - \chi_{\rm r}\,\rho_x}{\rho_{\rm m} - \rho_x\rho_y/\rho_{\rm m}}}. \end{cases} \tag{17}$$

By simple inspection of the above relations, it is straightforward to find that perfect transmission is not always possible, and this is illustrated in Fig. 4 where we report for $\rho_{\rm i} > \rho_{\rm m}$ and $\rho_{\rm i} < \rho_{\rm m}$ the ranges of $\chi_{\rm r}$ allowing for perfect transmission. It is worth noting that in the limit of thick films, we recover the expression of the Brewster angle $\theta_{\rm B}$ in (8) predicted by the effective medium model.

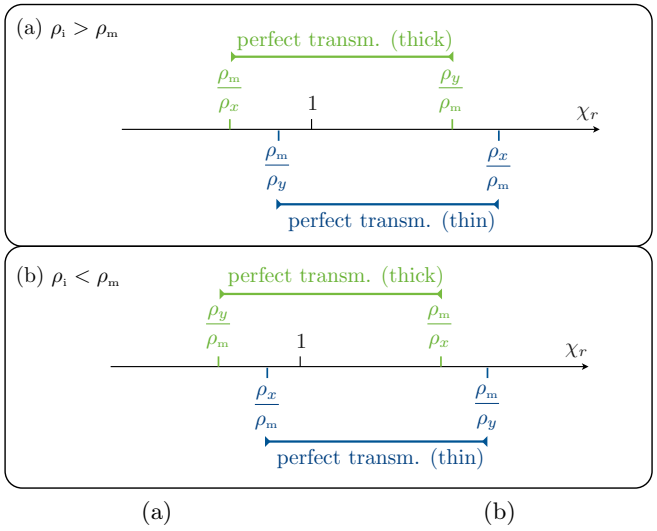

FIG. 4: Ranges of parameters for which perfect transmission is allowed in the limit of thick/thin film, from (17).

B. The case of sound-penetrable films

To begin with, we come back to the variation of θ^* reported in Fig. 2(a) and (b), where we considered a large contrast in the mass densities $\rho_{\rm i}/\rho_{\rm m} = 10^{-3}$. In (a), no contrast in the isentropic compressibility was considered, hence $\chi_{\rm r} = 1$; from (17) and Fig. 4, perfect transmission is expected to be possible for thin and thick films. Conversely, in (b), with $c_{\rm i} = 10c_{\rm m}$ we have $\chi_{\rm r} = 5.5$ from (15) and $(\rho_{\rm m}/\rho_x \simeq 2, \rho_{\rm m}/\rho_y \simeq 500)$ from (4); hence perfect transmission is expected to be possible for a thin film but not for a thick one. Also, in both cases, with $\rho_y < \rho_x$ in (17), θ^* is expected to increase when e/h increases since $\rho_{\rm i} < \rho_{\rm m}$ (the inverse is expected for $\rho_{\rm i} > \rho_{\rm m}$). These predictions are in agreement with the observations in Figs. 2(a) and (b).

More quantitatively, the effective interface model provides R in (12) reproducing the overall variations of $R_{\rm num}$ in Fig. 2(a) and (b) with an agreement of 1% and 7% respectively for $kh = 1$; the agreement is better for lower kh value with an overall lower reflection but the same values of θ^*. This accuracy is illustrated in Fig. 5 where we report a profile of $|R_{\rm num}|$ against θ along with the predictions of the classical model, (6) along with (7), and of the interface model, (12) along with (13) (with the interface parameters $\mathcal{B} = 0.037$, $\mathcal{C} = 0.441$ and $\mathcal{D} = 0.1$). We also report the variations in θ^* in very good agreement with that determined from the numerical computations, with $\theta^* \to 1.8°$ for $e/h \to 0$ (not shown on the plot) and $\theta^* \to \theta_{\rm B} = 45°$ for $e/h \to +\infty$ from (17).

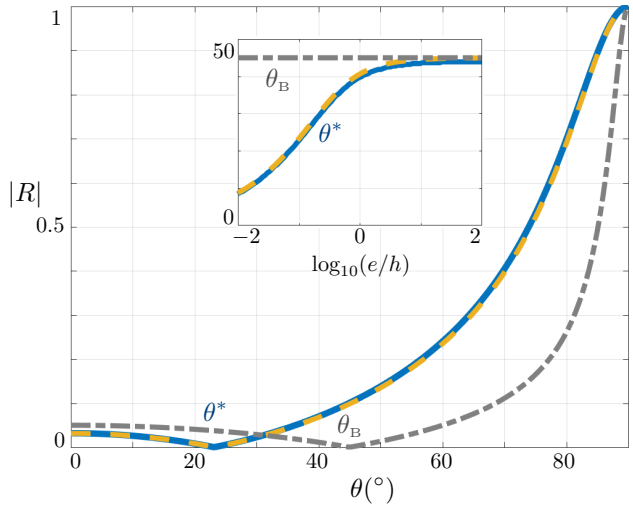

FIG. 5: Reflection coefficient against θ for a film with characteristics: $e/h = 0.1$, $\rho_{\rm m}/\rho_{\rm i} = 10^3$ and $\chi_{\rm m}/\chi_{\rm i} = 1$. Plain blue line shows $|R_{\rm num}|$ computed numerically, dotted yellow lines $|R|$ from the effective interface model, (12) with (13), and dashed grey line from the classical effective medium model, (6) along with (7). The inset shows the variations of θ^* against e/h.

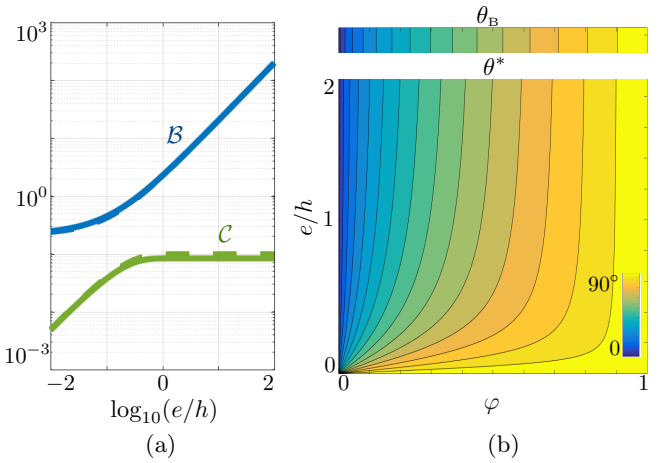

FIG. 6: Limiting case of rigid films – (a) Parameters $(\mathcal{B}_{\rm Neu}, \mathcal{C}_{\rm Neu})$ as a function of (e/h) $(\varphi = 0.5)$. The estimates in (18) are plotted in dashed lines. (b) Brewster angle θ^* against φ and e/h from (14) along with (18). The classical Brewster angle $\theta_{\rm B} = \arccos(1-\varphi)$ is reported for comparison.

C. Limiting case of sound-hard film

A case of practical interest in acoustic is that of sound-hard films, and the electromagnetic analog of metallic films for polarized waves in the far infrared. The effective interface model has been derived in [21, 23], and it yields to the same transmission conditions than in our Eq. (9) with interface parameters $(\mathcal{B}, \mathcal{C}, \mathcal{D})$ corresponding to $\rho_{\rm m}/\rho_{\rm i} = \chi_{\rm i}/\chi_{\rm m} = 0$. In this limit, we get from (4) that

$$\rho_{\rm m}/\rho_x = 0, \quad \chi_{\rm r} = \rho_{\rm m}/\rho_y = (1-\varphi),$$

and according to Fig. 4(a), this already tells us that a perfect transmission can occur for thin and thick films. But this does not tell much about $\mathcal{B}$ and $\mathcal{C}$ since the bounds in (16) leave us with $\frac{1}{1-\varphi}\frac{e}{h} \le \mathcal{B} \le +\infty$ and $0 \le \mathcal{C} \le (1-\varphi)\frac{e}{h}$. However, good estimates of $(\mathcal{B}, \mathcal{C})$ can be found (see [23]) with $\mathcal{D}$ still known explicitly, specifically we have

$$\begin{cases} \mathcal{B}_{\rm Neu} \simeq \dfrac{1}{(1-\varphi)}\dfrac{e}{h} - \dfrac{2}{\pi}\log\left(\cos\dfrac{\pi\varphi}{2}\right), \\ \mathcal{C}_{\rm Neu} \simeq \dfrac{\pi}{8}(1-\varphi)^2\left(1 - e^{-\frac{8e}{(1-\varphi)\pi h}}\right), \\ \mathcal{D}_{\rm Neu} = (1-\varphi)\dfrac{e}{h}, \end{cases} \tag{18}$$

which are compatible with their bounds; the estimates for $(\mathcal{B}_{\rm Neu}, \mathcal{C}_{\rm Neu})$ are reported in Fig. 6(a) together with their values computed numerically, which justifies their use. Reporting the above expressions of the effective parameters in (14) allows us to inspect the variations of θ^* with e/h and φ, see Fig. 6(b). Besides, from (18), we get simplified expressions of θ^* in the limits of thin and thick films

$$\begin{cases} \text{for thin films, } \cos\theta^* = \sqrt{\dfrac{-2}{\log\left(\cos\frac{\pi\varphi}{2}\right)}}\dfrac{e}{h} \to 0, \\ \text{for thick films, } \cos\theta^* = (1-\varphi), \end{cases} \tag{19}$$

and the Brewster angle for thick films again coincides with $\theta_{\rm B}$ given by the classical effective medium model see *e.g.* [5, 17]. By continuity, it follows that perfect transmission is always possible with a Brewster angle decreasing when e/h decreases, a fact observed in Fig. 2(c).

Fig. 7 reports a comparison between direct numerical

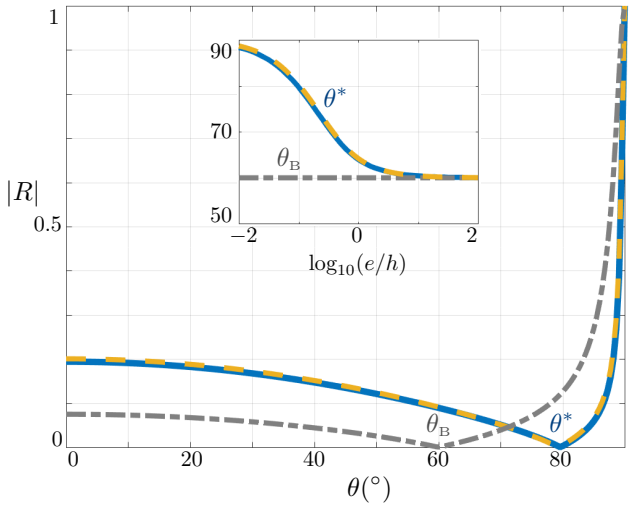

FIG. 7: Reflection $|R|$ against θ for a perforated rigid film, $e/h = 0.1$, $\varphi = 0.5$ and $kh = 1$. Same representation as in Fig. 5.

results and the predictions of the models for a profile of $|R|$ against θ (main plot for $e/h = 0.1$ and $\varphi = 0.5$), and for the variations of θ^* against e/h (inset, where $kh = 10^{-2}$ to avoid the Fabry -Perot resonances which take place for $ke = (n+1/2)\pi$, n integer). As for sound-penetrable films, a good accuracy of the effective interface model is observed. The overall agreement between R_{num} and Eq. (12) is of 5% for $kh = 1$ and $e/h \in (0, 1)$ as reported in Fig. 2(c), and as for the case of sound-penetrable film, the agreement is better for smaller kh value; a noticeable difference is that $e/h \to 0$ does not produces vanishing reflection but corresponds to a perforated rigid plate able to efficiently block the wave.

IV. CONCLUSION

We have studied the scattering properties of perforated films of variable thicknesses with a focus on thin films. The conditions under which perfect transmission is possible are modified when ultra thin devices are considered; in particular an extraordinary transmission observed for a thick film can disappear when reducing its thickness, and the reverse situation is possible as illustrated in Fig. 2(b). In all cases, a shift in the Brewster incidence θ^* has been exhibited : for film materials lighter than that of the surrounding matrix, θ^* increases with the thickness up to θ_{B}, for film material heavier, θ^* decreases with the thickness up to θ_{B}. The case of perforated sound-rigid films has been shown to be a limiting case of the sound-penetrable ones for a film material infinitely heavy; in this case, perfect transmission is always possible which is of particular interest since a perforated plate obtained for vanishing thickness remains very efficient to block the wave.

These features, and more generally the scattering properties of thin films, are accurately reproduced by an effective interface model which aims to capture the boundary layer effects largely dominant compared to that of wave propagation. Beyond the geometrical or compositional effects of the perforations, the thickness of the films offers a degree of freedom to tune its properties. Besides, it is a parameter of practical importance since it measures the compactness of the structure. With regards to the design of ultra-thin devices, such alternative models are of particular interest since they have their range of validity which complements that of the classical effective medium theory.

[1] S. G. Rodrigo, F. de León-Pérez and L. Martín-Moreno, Proceedings of the IEEE, **104**(12), 2288-2306 (2016).

[2] T.W. Ebbesen, H.J. Lezec, H.F. Ghaemi, T. Thio and P.A. Wolff, Nature **391** 667 (1998).

[3] M.H. Lu, X.K. Liu, L. Feng, J. Li, C.P. Huang, Y.F. Chen, T.Y. Zhu, S.N. Zhu and N.B. Ming, Phys. Rev. Lett., **99**(17), 174301 (2007).

[4] J. Christensen, L. Martin-Moreno and F.J. Garcia-Vidal,Phys. Rev. Lett., **101**(1), 014301 (2008).

[5] X.R. Huang, R.W. Peng and R.H. Fan, Phys. Rev. Lett., **105**(24), 243901 (2010).

[6] G. D'Aguanno, K.Q. Le, R. Trimm, A. Alù, N. Mattiucci, A.D. Mathias, S. Aközbek and M.J. Bloemer, Scientific reports, 2, 340 (2012).

[7] A.N. Norris and X. Su, Comptes Rendus Mécanique, **343**(12), 622-634 (2015).

[8] M. Edalatipour, A. Khavasi and K. Mehrany, JOSA B, **32**(6), 1202-1207 (2015).

[9] P. Wei, F. Liu, Z. Liang, Y. Xu, S.T. Chu and J. Li, EPL (Europhysics Letters), **109**(1), 14004 (2015).

[10] P. Peng, B. Xiao and Y. Wu, Phys. Lett. A, **378**(45), 3389-3392 (2014).

[11] A. Maurel, S. Félix and J.-F. Mercier, Phys. Rev. B, **88**(11), 115416 (2013).

[12] A. Akarid, A. Ourir, A. Maurel, S. Félix and J.-F. Mercier, Optics Lett., **39**(13), 3752-3755 (2014).

[13] T.K. Nguyen, P.T. Dang, I. Park and K.Q. Le JOSA B, **34**(3), 583-589 (2017).

[14] M. Molerón, M. Serra-Garcia and C. Daraio, New J. Phys., **18**(3), 033003 (2016).

[15] G. D'Aguanno, K. Q. Le, R. Trimm, A. Alù, N. Mattiucci, A. D. Mathias, N. Akozbek and M. J. Bloemer, Scientific reports, **2**, 340 (2012).

[16] D.-X. Qi, R.-H. Fan, R.-W. Peng, X.-R. Huang, M.-H. Lu, X. Ni, Q. Hu, and M. Wang, Appl. Phys. Lett. **101**, 061912 (2012).

[17] A. Alù, G. D'Aguanno, N. Mattiucci, and M. J. Bloemer, Phys. Rev. Lett. **106**, 123902 (2011).

[18] H.H. Sheinfux, I. Kaminer, Y. Plotnik, G. Bartal and M. Segev, Phys. Rev. Lett., **113**(24), 243901 (2014).

[19] A. Maurel and J.-J. Marigo, Phys. Rev. B, **98**(2), 024306 (2018).

[20] B. Delourme, K. Schmidt and A. Semin, Asymptotic Analysis, **97**(3-4), 211-264 (2016).

[21] J.-J. Marigo and A. Maurel, In Handbook of metamaterials properties (eds R.V. Craster, S. Guenneau), vol. 2, ch. 12, pp. 599-644. Singapore: World Scientific Publishing Company.

[22] J.-J. Marigo, A. Maurel, K. Pham and A. Sbitti, J. Elas., **128**(2), 265-289 (2017).

[23] J.-J. Marigo and A. Maurel, J. Acoust. Soc. Am., **140**(1), 260-273 (2016).

Appendix A: Effective parameters $(\mathcal{B}, \mathcal{C})$ and their bounds

In the jumps of pressure and normal velocity, three so-called interface parameters among which $(\mathcal{B}, \mathcal{C})$ have to

be determined numerically. They are defined as

$$\left\{\begin{array}{l} \mathcal{B} \equiv \dfrac{e}{h} + \left(\lim\limits_{y_1\to+\infty} Q_{\rm y} - \lim\limits_{y_1\to-\infty} Q_{\rm y} \right), \\ \mathcal{C} \equiv \dfrac{e}{h}\left(\varphi\dfrac{\rho_{\rm m}}{\rho_{\rm i}} + 1 - \varphi\right) + \displaystyle\int_{\Omega_\infty} {\rm d}\boldsymbol{\xi}\ \frac{\rho_{\rm m}}{\rho(\boldsymbol{\xi})}\frac{\partial Q_{\rm x}}{\partial \xi_x}(\boldsymbol{\xi}), \end{array}\right. \tag{A1}$$

with $\boldsymbol{\xi} = (\xi_x, \xi_y) = (x, y)/h$ a rescaled coordinate and $\varphi = \mathcal{S}_{\rm i}/h^2$ where $\mathcal{S}_{\rm i}$ is the surface of the perforated film. The parameter $\mathcal{D}$ is given explicitly and $(\mathcal{B}, \mathcal{C})$ are deduced from static problems set on $(Q_{\rm x}, Q_{\rm y})$, and satisfying for $\alpha = x, y$

$$\left\{\begin{array}{ll} {\rm div}\left[\dfrac{\rho_{\rm m}}{\rho}\nabla\left(Q_\alpha + \xi_\alpha\right)\right] = 0, & \\ Q_\alpha & \text{continuous} \\ \dfrac{\rho_{\rm m}}{\rho}\,\partial_n\left(Q_\alpha + \xi_\alpha\right) & \\ \lim\limits_{\xi_y\to\pm\infty} \nabla Q_\alpha = \mathbf{0}. & \end{array}\right.$$

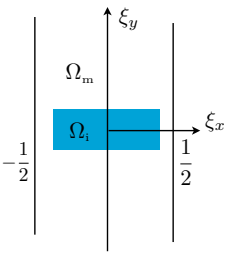

FIG. 8: Elementary problems on (Q_x, Q_y) set in $\Omega = \Omega_{\rm i} \cup \Omega_{\rm m} = (-1/2, 1/2) \times (-\infty, \infty)$ used to calculate $(\mathcal{B}, \mathcal{C})$, Eqs. (A1).

It is worth noting that these problems have several advantages (i) they are static, (ii) they depend on the contrast in mass density only, the contrast in the sound speed being encapsulated explicitly in $\chi_{\rm r}$, (iii) they are set in a non-dimensional geometry (with a reference length h). As such $(\mathcal{B}, \mathcal{C})$ hold for a large family of settings; besides, once they are determined, the effective problem can be solved in the transient as in the harmonic regime for any kind of source and any radiation or boundary conditions.

1. Upper bound for $\mathcal{B}$

Determining an upper bound for $\mathcal{B}$ requires to invoke the Thomson principle (a similar calculation can be found in [22] for the determination of the upper bound of $\mathcal{C}$). It is based on the equivalence between the problem on $Q_{\rm y}$ and the problem of energy minimization for $\boldsymbol{U} = (\rho_{\rm m}/\rho)\,\boldsymbol{\nabla}(Q_{\rm y} + \xi_y)$ which reads

$$\begin{array}{l} E(\boldsymbol{U}) \le E(\tilde{\boldsymbol{U}}), \\ \text{with} \quad E^*(\tilde{\boldsymbol{U}}) = \dfrac{1}{2}\displaystyle\int_\Omega {\rm d}\boldsymbol{\xi}\ \frac{\rho}{\rho_{\rm m}}\left|\tilde{\boldsymbol{U}} - \frac{\rho_{\rm m}}{\rho}\boldsymbol{e}_y\right|^2, \end{array} \tag{A2}$$

for any admissible field $\tilde{\boldsymbol{U}}$ with $\tilde{\boldsymbol{U}}\cdot\mathbf{n}$ continuous, ξ_x-periodic in Ω and satisfying ${\rm div}\tilde{\boldsymbol{U}} = 0$, $\tilde{\boldsymbol{U}} \to \boldsymbol{e}_y$ for $\xi_y \to \pm\infty$. We start by linking $E(\boldsymbol{U}) = \frac{1}{2}\int_\Omega {\rm d}\boldsymbol{\xi}\ \frac{\rho_{\rm m}}{\rho}|\boldsymbol{\nabla}Q_{\rm y}|^2$ to $\mathcal{B}$; we use that $0 = \int_\Omega {\rm d}\boldsymbol{\xi}\ (Q_{\rm y} - \xi_y)\ {\rm div}\left[\frac{\rho_{\rm m}}{\rho}\boldsymbol{\nabla}\left(Q_{\rm y} + \xi_y\right)\right]$, from which making use of the boundary conditions

$$\int_\Omega {\rm d}\boldsymbol{\xi}\ \frac{\rho_{\rm m}}{\rho}|\boldsymbol{\nabla}Q_{\rm y}|^2 = \int_\Omega {\rm d}\boldsymbol{\xi}\ \frac{\rho_{\rm m}}{\rho} + \lim_{\xi_m\to+\infty}\left[Q_{\rm y} - \xi_y\right]_{-\xi_m}^{+\xi_m}. \tag{A3}$$

Both terms on the right hand side diverge in the above expression, but not their sum; specifically, we have

$$\left\{\begin{array}{l} \displaystyle\int_\Omega {\rm d}\boldsymbol{\xi}\ \frac{\rho_{\rm m}}{\rho} = 2\lim_{\xi_m\to+\infty}\xi_m - \varphi\left(1 - \frac{\rho_{\rm m}}{\rho_{\rm i}}\right), \\ \displaystyle\lim_{\xi_m\to+\infty}\left[Q_{\rm y} - \xi_y\right]_{-\xi_m}^{+\xi_m} = (\mathcal{B}^+ - \mathcal{B}^-) - 2\lim_{\xi_m\to+\infty}\xi_m, \end{array}\right. \tag{A4}$$

where $\mathcal{B}^\pm = \lim\limits_{y_1\to\pm\infty} Q_{\rm y}$. Hence

$$E(\boldsymbol{U}) = \frac{1}{2}\left[(\mathcal{B}^+ - \mathcal{B}^-) - \varphi\frac{e}{h}\left(1 - \frac{\rho_{\rm m}}{\rho_{\rm i}}\right)\right]. \tag{A5}$$

It is now sufficient to choose the simple admissible field $\tilde{\boldsymbol{U}} = \boldsymbol{e}_y$, which provides $E(\tilde{\boldsymbol{U}}) = \frac{\varphi e}{2h}\frac{\rho_{\rm i}}{\rho_{\rm m}}\left(1 - \frac{\rho_{\rm m}}{\rho_{\rm i}}\right)^2$ and to invoke (A2) to get that $\mathcal{B} = (\mathcal{B}^+ - \mathcal{B}^-) + \frac{e}{h}$ in (A1) satisfies

$$\mathcal{B} \le \frac{e}{h}\left(\varphi\frac{\rho_{\rm i}}{\rho_{\rm m}} + 1 - \varphi\right). \tag{A6}$$

2. Upper bound for $\mathcal{C}$

The upper bound on $\mathcal{C}$ is straightforward. It is sufficient to use that $\displaystyle\int_\Omega {\rm d}\boldsymbol{\xi}\ Q_{\rm x}\ {\rm div}\left[\frac{\rho_{\rm m}}{\rho}\boldsymbol{\nabla}\left(Q_{\rm x} + \xi_x\right)\right] = 0$, from which

$$\int_\Omega {\rm d}\boldsymbol{\xi}\ \frac{\rho_{\rm m}}{\rho}\frac{\partial Q_{\rm x}}{\partial \xi_x}(\boldsymbol{\xi}) = -\int_\Omega {\rm d}\boldsymbol{\xi}\ \frac{\rho_{\rm m}}{\rho}|\boldsymbol{\nabla}Q_{\rm x}|^2 \le 0, \tag{A7}$$

where we used the boundary conditions on $Q_{\rm x}$. With $\mathcal{C}$ defined in (A1), we get the upper bound

$$\mathcal{C} \le \frac{e}{h}\left(\varphi\frac{\rho_{\rm m}}{\rho_{\rm i}} + 1 - \varphi\right). \tag{A8}$$